Note: This is a paper submitted for publication. Contents of this paper should not be quoted or referred to without permission of the author(s).

Submitted to:

Physics of Plasmas

Comparison of toroidal rotation velocities of different impurity ions in the DIII-D tokamak*

L. R. Baylor[a], K.H. Burrell[#], R. J. Groebner[#], W.A. Houlberg,
D.P. Ernst*, M. Murakami, M. R. Wade

Oak Ridge National Laboratory, Oak Ridge, TN 37831-8071

[a)] Electronic mail: BaylorLR@ornl.gov;

[#]General Atomics, San Diego, CA

** Massachusetts Institute of Technology, Cambridge, MA*

The submitted manuscript has been authored by a contractor of the U.S. Government under contract No. DE-AC05-00OR22725. Accordingly, the U.S. Government retains a nonexclusive, royalty-free license to publish or reproduce the published form of this contribution, or allow others to do so, for U.S. Government purposes.

December 8, 2003

Prepared by the
OAK RIDGE NATIONAL LABORATORY
Managed by
UT-BATTELLE, LLC, for the
U.S. DEPARTMENT OF ENERGY
Under Contract No. DE-AC05-00OR22725

*Work supported by U.S. Department of Energy under Contract Nos. DE-AC03-99ER54463, DE-FC02-99ER54512, and DE-AC05-00OR22725.

Comparison of toroidal rotation velocities of different impurity ions in the DIII-D tokamak*

L.R. Baylor, K.H. Burrell[#], R. J. Groebner[#], W.A. Houlberg,
D.P. Ernst*, M. Murakami, M. R. Wade
Oak Ridge National Laboratory, Oak Ridge, Tennessee
[#]*General Atomics, San Diego, California*
* *Massachusetts Institute of Technology, Cambridge, Massachusetts*

Measurements of the relative toroidal rotation velocities of low Z impurity ions has been made in DIII-D plasmas that have a strong core pressure gradient and reduced anomalous transport. They show that the differences in toroidal rotation velocities agree with predictions of neoclassical transport theory. The toroidal rotation velocities are measured via charge exchange recombination (CER) spectroscopy of the impurity species. Taking into account the non-negligible effect of energy dependent charge exchange cross sections, quantitative agreement is found between the measured and predicted difference in toroidal rotation velocities, including the strong Z dependence.

PACS numbers: 52.55.-s, 52.25.Fi, 52.25.Vy

*Work supported by U.S. Department of Energy under Contract Nos. DE-AC03-99ER54463, DE-FC02-99ER54512, and DE-AC05-00OR22725.

1. INTRODUCTION

The shear in plasma *ExB* rotation has been shown to be very important in the stabilization of turbulence in high temperature tokamak plasmas [1]. In plasmas with unbalanced neutral beam injection (NBI) the toroidal rotation is a major contributor to the *ExB* rotation, therefore it is critical to have a good measure of the toroidal rotation in order to understand how to control the turbulence driven transport. The toroidal rotation velocity is usually measured in tokamaks with charge exchange recombination (CER) spectroscopy of an impurity species [2]. The theory of collisional transport of energy and particles in toroidal confinement devices (so-called neoclassical transport) has been well developed in magnetic fusion research since the early 1980s [3,4]. This theory predicts the difference in the rotation velocity between various plasma ion species, which is largely determined by the difference in their pressure gradients $\nabla P_i/Z_i$, where Z_i is the nuclear charge for species i [4]. In this paper, we present experimental confirmation of this prediction.

On the DIII-D tokamak the emission lines of the C^{5+} intrinsic impurity are routinely used to measure the toroidal rotation velocity by the Doppler shifted emission where the donor electrons for the CER process are provided by neutral beam injection (NBI) [2,5,6]. The direct measurement of the deuterium main species rotation velocity is not possible in neutral beam heated plasmas due to the D_α line being seriously affected by thermal emission from the plasma edge and by Doppler shifted emission from the NBI ions. Accordingly, we test the theory by measuring the rotation velocities of several impurity ions, He, C, and Ne. Detailed analysis of the emission line spectra that takes into account the energy dependent charge exchange cross section is required to obtain highly accurate ion temperature and rotation measurements [7] for this study.

Indirect observations of a difference in the main ion species and impurity species toroidal rotation velocities have been reported in previous work. In TFTR, a notch measured in the carbon rotation profile in supershot plasmas was examined by Ernst, et al. [8] who inferred that anomalous radial momentum diffusion would lead to a monotonic rotation profile for the bulk deuterium species while parallel heat friction resulted in the notch in the impurity rotation profile. A comparison of the carbon toroidal rotation profile with MHD mode rotation velocities of the main ion species was made in JET by Testa, et al.[9], where the difference in the velocities was in reasonable agreement with neoclassical calculations.

In this paper we report the first direct simultaneous measurement of multiple ion species toroidal rotation profiles across the entire plasma radius in a tokamak plasma. The theoretical expectations for the difference in toroidal rotation from collisional neoclassical theory are presented in Sec. II. In Sec. III of this paper we describe the experimental configuration and measurement technique used. In Sec. IV we present the results of experiments comparing the toroidal rotation velocities of multiple ion species. Finally in Sec. V we present a summary of our main conclusions and discuss the implications of these experimental results on transport.

II. THEORY

The radial electric field in a plasma is related to the fluid flow velocity, V_i, and pressure gradient of each species, ∇P_i, through the radial force balance, $n_i e_i (E_r + V_i x B) = \nabla P_i$ [1,3], where n_i is the density, e_i is the charge and B is the magnetic field. In terms of the toroidal and poloidal components of the magnetic field and flow velocity, the local radial electric field for any ion species is:

$$E_r = \frac{\nabla P_i}{n_i e Z_i} - V_{\theta,i} B_\phi + V_{\phi,i} B_\theta \quad , \tag{1}$$

where the subscripts θ and ϕ designate the poloidal and toroidal rotation directions respectively and ∇ indicates the gradient in the radial direction. Since the radial electric field is a local plasma parameter independent of the species it is possible to write the difference in the toroidal rotation velocity of two species as:

$$\Delta V_{\phi,12} = \left(\frac{\nabla P_2}{Z_2 e n_2} - \frac{\nabla P_1}{Z_1 e n_1} \right) B_\theta^{-1} + \left(V_{\theta,1} - V_{\theta,2} \right) \frac{B_\phi}{B_\theta} , \tag{2}$$

where subscripts 1 and 2 refer to the two ion species being considered. For the case where the poloidal velocities and their difference are small, the dominant contribution is from the ∇P difference term. For high Z impurities, the effect of the pressure gradient terms is reduced because of the Z dependence shown in Eqn.2.

The poloidal rotation velocity can be determined from the parallel force and heat flux balances in neoclassical theory of transport as summarized in the review by Hirshman and Sigmar [4]. It is strongly damped by the poloidal variation of the magnetic field, responds to the thermodynamic forces (pressure, temperature and potential gradients) on an ion-ion collision timescale, and is a function of the plasma collisionality. Determination of the poloidal velocity in a tokamak plasma consisting of multiple ion species requires solution of the coupled force and heat flux balance equations for each charge state of each species. The NCLASS code [10] implements the velocity moment formalism of Hirshman and Sigmar [4] to numerically calculate these neoclassical flows and other transport properties in axisymmetric plasmas consisting of an arbitrary number of species. It uses expressions for the viscosity that are continuous over all collisionality regimes and aspect ratios to calculate the poloidal flows. NCLASS determines a neoclassical poloidal rotation flux function for each species, $\hat{u}_{\theta,i} = \langle u_i \cdot \nabla\theta \rangle / \langle B \cdot \nabla\theta \rangle$, from which the local neoclassical poloidal rotation can be determined, $V_{\theta,i} = B_\theta \hat{u}_{\theta,i}$. The

result is a more rigorous calculation than the analytic approximations used in the two ion species model developed by Kim et al. [11]. NCLASS is called by a front-end code named FORCEBAL that prepares input to NCLASS from MHD equilibrium solutions and profile measurements, then outputs the radial electric field and its pressure and rotation components for each species.

The validity of the expected rotation velocity difference in Eq.(2) has been experimentally verified in the edge plasma region on the DIII-D tokamak [12] for a helium plasma using helium, carbon, and boron rotation measurements. In that work the computed difference in toroidal rotation velocities between the different species was found to agree with theory except in the steep gradient region at the very edge of the H-mode plasma. The ordering of standard neoclassical theory breaks down when the gradient scale lengths or proximity to the plasma boundary are comparable to the ion poloidal gyroradius, conditions that are typical of the H-mode pedestal at the plasma edge and at strong internal barriers concomitant with strongly reversed central shear.

III. EXPERIMENT

In order to maximize the difference in toroidal rotation velocities, Eq. (2) predicts that it is desirable to measure the rotation velocities in plasmas with a strong pressure gradient. In DIII–D, quiescent High-confinement mode plasmas with a double transport barrier (QDB) [13], are characterized with a strong pressure gradient in the core plasma with reduced turbulent transport thus making a good target discharge for this study. The time evolution of a typical QDB deuterium discharge is shown in Fig. 1. NBI directed counter to the plasma current direction is the dominant heating method for these discharges and it provides a strong angular momentum source to drive the toroidal rotation. The QDB phase of the discharge persists for well over 1 sec. making it possible

to inject trace impurities with a gas valve and allow the impurities to equilibrate in the plasma before making the profile measurements. Carbon is the dominant impurity and is intrinsically in the plasma due to the graphite plasma facing components. Two very similar QDB discharges are used in this study, one with trace helium gas injection and the other with trace neon injection during the QDB phase. The density and temperature profiles measured by Thomson scattering for the electrons and by CER for the ions are shown in Fig. 2 for one of these discharges at the time of analysis (3.5s). The ion temperature profile is that measured for C^{6+} and shows strong peaking with a high edge pedestal value typical of the QDB plasmas. The impurity density profiles are shown in Fig. 3a and 3b for the He and Ne gas injection cases respectively. The impurity density profiles are determined by a calculation based on the brightness of the CER signal and calculated beam deposition profiles, which depend on the plasma temperature and density profiles and known beam characteristics [14]. The deuterium density profile is calculated from the electron density profile by subtracting the impurity density profiles and the fast ion density profile, which is calculated using the TRANSP code [15]. The plasma equilibrium is calculated with the EFIT code [16] and is used to fit all of the profile data onto a normalized toroidal flux grid (ρ). The safety factor (q) profile as determined from motional Stark effect data [17] and EFIT shows a weak negative shear region in the plasma core inside of ρ = 0.3 and a safety factor of 3.9 near the plasma separatrix location (ρ = 0.95).

The CER diagnostic during this experiment used two measurement systems, one a RETICON linear array and the other a charge-coupled device (CCD) detector. Each was mounted on spectrometers that observe the spectral light from the charge exchange process through collimated tangential views. Eight channels across the minor radius were measured by each system. In these experiments one of the tangential viewing cameras was tuned to the intrinsic C VI 529.1 nm line while the other was tuned to either the Ne X 524.9 nm or He II 468.5 nm lines depending on which trace impurity was injected.

These lines provided measurements of the C^{6+}, Ne^{10+} and He^{2+} ions, respectively. A wavelength calibration of the CCD detectors is performed after every plasma discharge with a neon discharge lamp in order to precisely define the Doppler shift of the spectral lines [18]. The spectral resolution of these detectors is 0.01 to 0.02 nm/pixel and by taking into account the instrumental broadening of the spectrometers it is possible to obtain sub pixel resolution. The error bars shown in the CER measurement profile plots are determined from standard propagation of errors from photoelectron statistics. Systematic errors from sources such as fiducial line positions and beam attenuation calculations are believed to lead to less than ~10 km/s uncertainty in rotation velocity. Modulation of the neutral beams at a frequency of 50 Hz was used to simplify the analysis of the measured CER spectra by allowing discrimination of the beam induced signal from the background radiation.

The spectrum produced by CER of a thermal population of plasma ions is to lowest order a shifted Gaussian in wavelength space. The cross section for the charge exchange process varies as a function of relative velocity between ions and beam atoms, thus the spectrum is modified from a Gaussian and can lead to systematic offsets of temperature and rotation velocity [16] when a Gaussian fit to the data is used. The CERFIT analysis code [7] has been modified to include the energy dependent cross section using the analytic cross sections from von Hellerman [19] to accurately determine the ion temperatures and rotation velocities. Errors in temperature as large as 2 keV and in rotation of 60 km/s are possible in QDB plasmas if the energy dependent cross section is not taken into account.

Profile data is input with an EFIT calculated equilibrium to the FORCEBAL code, which computes the radial force balance electric field in Eq. 1 from the C^{6+} input data. The NCLASS code is called by FORCEBAL to obtain the neoclassical poloidal rotation flux function to determine the neoclassical poloidal rotation velocity used in the electric field calculation since no direct measurements of it were available for the discharges

analyzed in this paper. Local toroidal rotation velocities of the injected trace impurity species of interest are then reconstructed using the input density profiles for these impurities as described in Sec. II.

IV. RESULTS

The measured T_i and V_ϕ profiles from the CER line broadening measurement of the trace impurities for the discharges with the helium gas injection and neon gas injection are shown in Figs. 4 and 5 respectively and are compared with the measured carbon profiles in the same discharges. The T_i profile agreement between the carbon and trace impurity species is within the error bars of the measurement for both helium and neon as expected and this gives us confidence that the diagnostic measurements are providing accurate results. The CER toroidal rotation velocity measurement based on the line shift shows a distinct difference between the carbon and helium profiles shown in Fig. 4, but a very small difference between the carbon and neon profiles shown in Fig. 5. The error bars on the rotation measurement from statistical errors are significantly less than the difference between the carbon and helium rotation shown in Fig. 4.

The calculated radial electric field and its terms for carbon from Eq. 1 are shown in Fig. 6 for the discharge with the helium gas injection. The dominant term for the radial electric field in this QDB plasma is by far the toroidal rotation term due to the strong torque provided by the unidirectional neutral beams. A highly anomalous poloidal rotation velocity would be required to make a significant impact on the radial electric field determination. The electric field terms for the main and trace impurity ion species in the plasma are qualitatively not very different from these shown for carbon.

The theoretical predictions of the helium and neon toroidal rotation velocities for these cases were made with the FORCEBAL code using the carbon rotation measurements as input values and are shown in Figs. 7 and 8. The data points from the

impurity species measurements (He or Ne) are shown along with a profile fit to the carbon toroidal rotation velocity data points. In both cases the calculated rotation velocity for the deuterium main ion species is also shown. The calculated deuterium toroidal rotation profile shows a reversal in the rotation direction near the edge of the plasma. The measured helium rotation profile is also calculated to reverse directions near the edge, and measurement channels outside the last closed flux surface do confirm this expected feature.

The agreement between the measured and calculated toroidal rotation velocities is quite good in both the helium and neon impurity cases. Only one data point in the helium profile shows any appreciable difference with the calculation. This may be due to some unknown systematic error for this channel that is not currently understood. As expected from the radial force balance, the neon and carbon toroidal rotation velocities are similar due to the inverse Z dependence in the pressure gradient term. The lighter species such as helium and deuterium are not rotating nearly as fast as the higher Z species such as carbon. For a case where the NBI is codirectional with the plasma current, the ion toroidal rotation is in the opposite direction of the counter NBI case and the low Z species typically rotate faster than the higher Z species.

The toroidal Mach number ($M = V_\phi / c_s = V_\phi / \sqrt{\gamma 2kT_e / m_i}$) of the different ion species has been calculated for these discharges under study and their profiles are shown in Fig. 9. We find that for all species the toroidal Mach number is less than unity (subsonic) except for neon in the very core of the discharge where it reaches a value of 1.2 at the magnetic axis. The neoclassical formalism is only valid in the subsonic regime, thus these measurements are made where Mach number and magnetic shear are not expected to adversely affect the rotation comparison with neoclassical theory.

V. SUMMARY AND CONCLUSIONS

In conclusion, we have made the first direct toroidal rotation velocity profile and ion temperature measurements of multiple ion species with CER across the entire plasma radius simultaneously in a tokamak plasma. Careful analysis of the CER spectra taking into account the energy dependent cross section was performed. Ion temperature profile measurements from the different impurities agree within the experimental error bars. A clear difference between toroidal rotation velocities of low-Z impurities are observed in QDB plasmas in the DIII–D tokamak with the magnitude of the difference decreasing with higher Z. In this study where the magnetic shear is weak and toroidal rotation velocities are subsonic, very good agreement is found between the measured rotation profiles and those calculated using the radial force balance and neoclassical theory. Thus the difference in toroidal rotation velocities is believed to be dominated by neoclassical processes.

These results and indirect evidence from MHD mode rotation measurements in JET [9] and the non-monotonic impurity toroidal rotation profile first observed in TFTR [8] support the validity of the predicted rotation speeds for the main ion (deuterium) species. The difference between the measured impurity rotation velocity and the main ion rotation velocity can be substantial and therefore one should be careful in using quantitative results from impurity rotation measurements and applying them to the bulk plasma. In the future, detailed measurement and analysis of the poloidal rotation velocity is needed to determine whether it is also consistent with neoclassical theory.

ACKNOWLEDGMENTS

This work was supported by the Oak Ridge National Laboratory managed by UT-Battelle, LLC for the U.S. Department of Energy under Contract No. DE-AC05-00OR22725 and also supported under contracts DE-AC03-99ER54463, and DE-FC02-99ER54512.

1. K.H. Burrell *et al.*, Phys. Plasmas **5**, 1878 (1998).

2. Isler, R.C., Plasma Phys. Control. Fusion **36**, 171 (1994).

3. S.I. Braginskii, in Reviews of Plasma Physics Vol. 1, ed. M. A. Leontovich, Consultants Bureau, New York (1965), 205.

4. S.P. Hirshman and D.J. Sigmar, Nucl. Fusion **21**, 1079 (1981).

5. R. J. Fonck, D. S. Darrow, and K. P. Jaehnig, Phys. Rev. A 29, 29 (1984)

6. P. Gohil, et al., *Proceedings of 14th Symposium*, IEEE 1199 (1991).

7. R.J. Groebner, *et al*., Bull. Am. Phys. Soc. **47**, 9, 302 (2002).

8. D.R. Ernst, *et al*., Phys. Plasmas **5**, 665 (1998).

9. D. Testa, C. Giroud, A. Fasoli, K.-D. Zastrow, EFDA-JET Team, Phys. Plasmas **9**, 243 (2002).

10. W.A. Houlberg *et al.*, Phys. Plasmas **4**, 3230 (1997).

11. Y. Kim, P. Diamond, and R. Groebner, Phys. Fluids B **3**, 2050 (1991).

12. J. Kim, K.H. Burrell, P. Gohil, *et al*., Phys. Rev. Lett. **72**, 2199 (1994).

13. K.H. Burrell, *et al.*, Phys. Plasmas **8**, 2153 (2001).

14. R.C. Isler, *et al.* , Phys. Rev. A **24**, 2701 (1981).

15. R.J. Hawryluk, *Proc. Course in Physics Close to Thermonuclear Conditions*, Varenna, (1979) (*Commission of the European Physical Society, Brussels, 1980*) vol I, p 19.

16. L. L. Lao, J. R. Ferron, R. J. Groebner, W. Howl, H. St. John, E. J. Strait, and T. S. Taylor,Nucl. Fusion **30**, 1035 (1990).

17. B.W. Rice, D.G, Nilson, K.H. Burrell, L.L. Lao, Rev. Sci. Instrum. **70**, 815 (1999).

18. P. Gohil, et al., Rev. Sci. Instrum. **70**, 878 (1999).

19. M. Von Hellerman, Plasma Phys. Control. Fusion **37,** 71 (1995) .

11

LIST OF FIGURE CAPTIONS

Fig. 1. Temporal evolution of the plasma current, NBI power, normalized beta, line-averaged density, divertor Dα emission, and impurity gas injection in a QDB–mode plasma in DIII–D. Negative plasma current indicates counter neutral beam injection.

Fig. 2. Radial profiles of (a) electron density n_e, deuteron density n_D, carbon density n_C and (b) ion temperature T_i, electron temperature T_e at the analysis time in the QDB-mode plasma with helium injection from Fig. 1.

Fig. 3. Impurity density profiles for the QDB-mode discharges with intrinsic carbon and injected (a) helium or (b) neon gas.

Fig. 4. Charge exchange recombination spectrometry measurements of (a) ion temperature profiles and (b) toroidal rotation profiles for carbon and helium at the same time in the discharge.

Fig. 5. Charge exchange recombination spectrometry measurements of (a) ion temperature profiles and (b) toroidal rotation profiles for carbon and neon at the same time in the discharge.

Fig. 6. Profiles of the radial electric field (E_{tot}) and its components from Eq. 1 for the carbon species in the QDB-mode discharge with helium injection. $E_{\nabla P}$ is the pressure gradient component, $E_{V\theta}$ is the poloidal rotation component, and $E_{V\phi}$ is the toroidal rotation component.

Fig. 7. Profiles of the calculated helium and deuterium toroidal rotation compared with the measured helium and carbon toroidal rotation profiles.

Fig. 8. Profiles of the calculated neon and deuterium toroidal rotation compared with the measured neon and carbon toroidal rotation profiles.

Fig. 9. Calculated toroidal Mach number profiles for the carbon, helium, neon (different but similar discharge),and deuterium species.

12

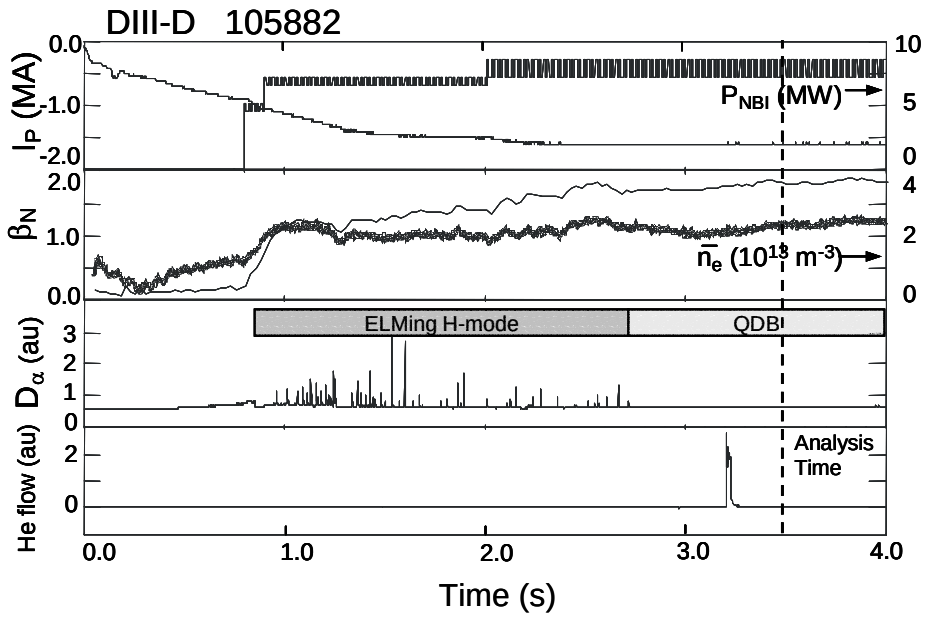
DIII-D 105882
I_P (MA)
P_{NBI} (MW)
β_N
$\bar{n}_e$ (10^{13} m^{-3})
ELMing H-mode
QDB
D_α (au)
He flow (au)
Analysis Time
Time (s)

Figure 1

13

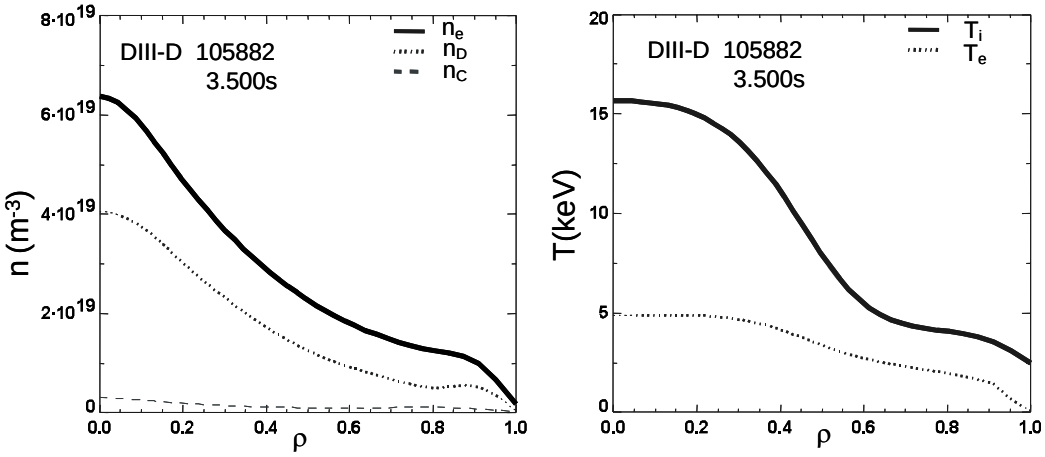
DIII-D 105882
3.500s
n_e
n_D
n_C
n (m^{-3})
8·10^{19}
6·10^{19}
4·10^{19}
2·10^{19}
0
0.0
0.2
0.4
0.6
0.8
1.0
ρ
DIII-D 105882
3.500s
T_i
T_e
T(keV)
20
15
10
5
0
0.0
0.2
0.4
0.6
0.8
1.0
ρ

Figure 2

14

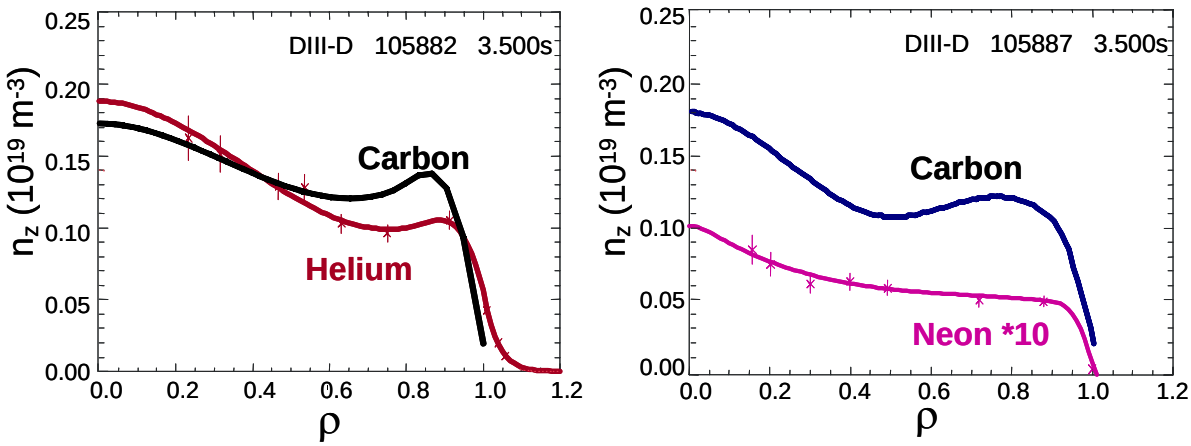
DIII-D 105882 3.500s
Carbon
Helium
n_z (10^{19} m^{-3})
ρ
DIII-D 105887 3.500s
Carbon
Neon *10
n_z (10^{19} m^{-3})
ρ

Figure 3

15

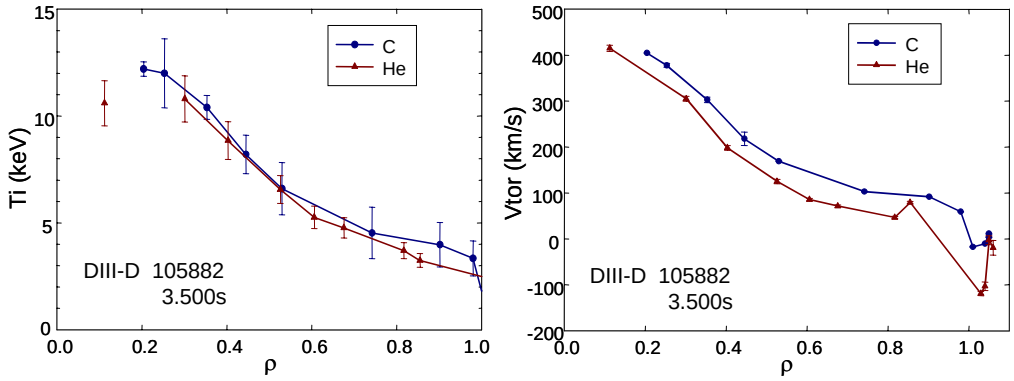
Ti (keV)
ρ
C
He
DIII-D 105882
3.500s
Vtor (km/s)
ρ
C
He
DIII-D 105882
3.500s

Figure 4

16

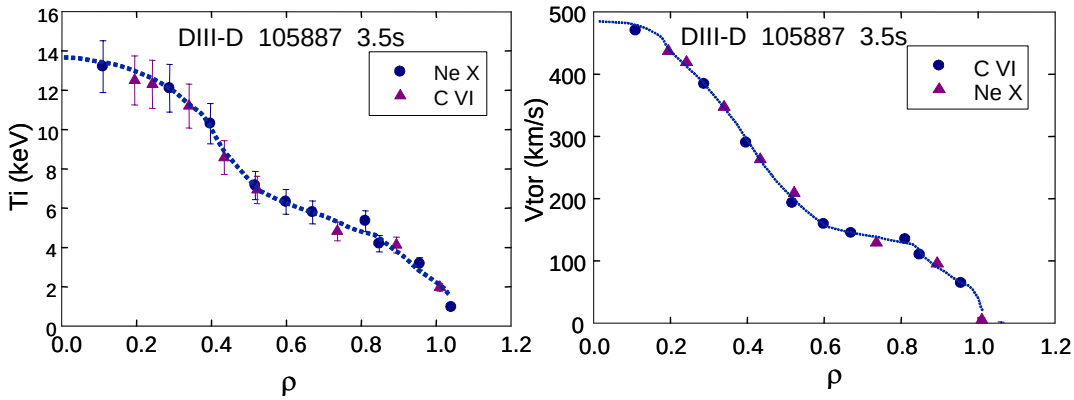
DIII-D 105887 3.5s
Ne X
C VI
Ti (keV)
ρ
DIII-D 105887 3.5s
C VI
Ne X
Vtor (km/s)
ρ

Figure 5

17

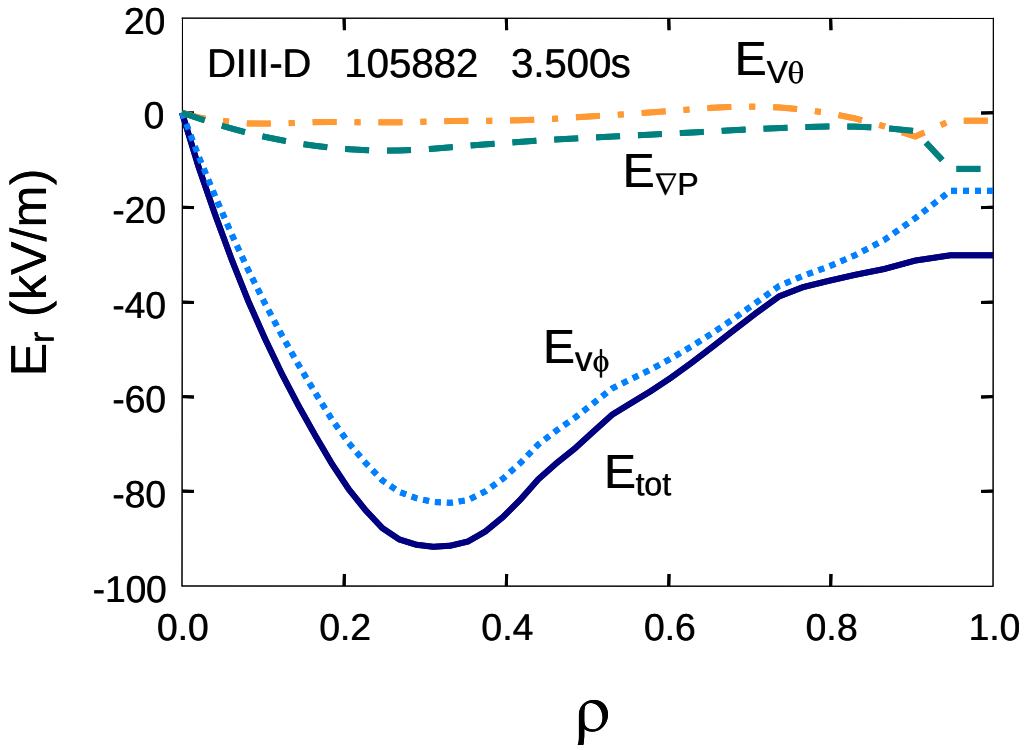
DIII-D 105882 3.500s
$E_{V\theta}$
$E_{\nabla P}$
$E_{V\phi}$
E_{tot}
E_r (kV/m)
ρ
20
0
-20
-40
-60
-80
-100
0.0
0.2
0.4
0.6
0.8
1.0

Figure 6

18

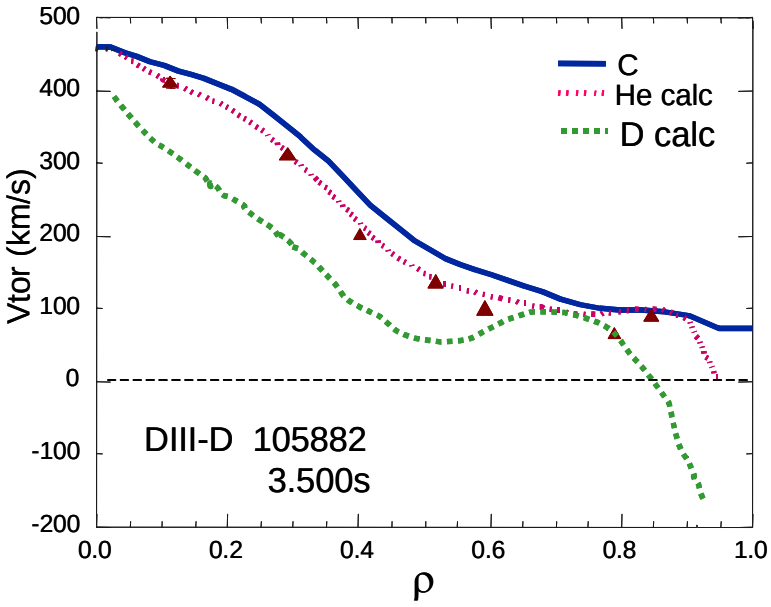
500
400
300
200
100
0
-100
-200
Vtor (km/s)
0.0
0.2
0.4
0.6
0.8
1.0
ρ
C
He calc
D calc
DIII-D 105882
3.500s

Figure 7

19

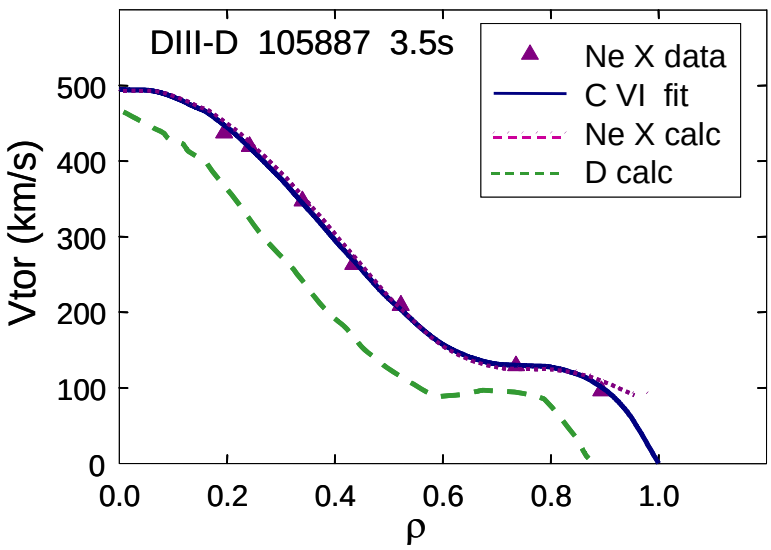
DIII-D 105887 3.5s
Ne X data
C VI fit
Ne X calc
D calc
Vtor (km/s)
500
400
300
200
100
0
0.0
0.2
0.4
0.6
0.8
1.0
ρ

Figure 8

20

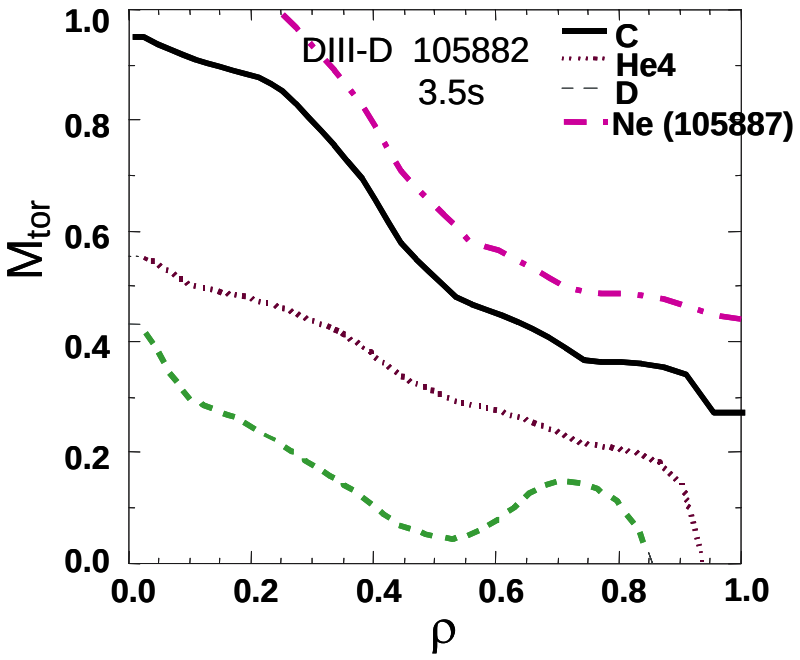
DIII-D 105882
3.5s
C
He4
D
Ne (105887)
1.0
0.8
0.6
0.4
0.2
0.0
0.0
0.2
0.4
0.6
0.8
1.0
M_{tor}
ρ

Figure 9

21